Extreme Mechanics Letters 35 (2020) 100640

Contents lists available at ScienceDirect

Extreme Mechanics Letters

journal homepage: www.elsevier.com/locate/eml

Parameters analysis and optimization of a typical multistable mechanical metamaterial

Jian Hua [a], Hongshuai Lei [b,c,d,*], Cun-Fa Gao [a,*], Xiaogang Guo [b,c,*], Daining Fang [b,c]

[a] State Key Laboratory of Mechanics and Control of Mechanical Structures, Nanjing University of Aeronautics and Astronautics, Nanjing 210016, PR China
[b] Beijing Key Laboratory of Lightweight Multi-functional Composite Materials and Structures, Beijing Institute of Technology, Beijing 100081, PR China
[c] State Key Laboratory of Explosion Science and Technology, Beijing Institute of Technology, Beijing 100081, PR China
[d] State Key Laboratory for Strength and Vibration of Mechanical Structures, School of Aerospace Engineering, Xi'an Jiaotong University, Xi'an 710049, PR China

ARTICLE INFO

Article history:
Received 18 December 2019
Received in revised form 29 January 2020
Accepted 29 January 2020
Available online 30 January 2020

Keywords:
Metastructure
Multi-stability
Peak force
Energy absorption efficiency

ABSTRACT

In this work, mechanical properties of a typical multistable mechanical metamaterial were analyzed in detail. When the maximum strain of the structure was kept constant during deflection, it was found that the largest peak force and best energy absorption efficiency can be obtained by adjusting its geometrical parameters. The influence of parameters on the force–displacement curve of the unit cell under large deformation is also discussed. Moreover, to further verify the conclusions from theoretical and finite element analysis (FEA), we experimentally investigated the mechanical performances of two different multilayer structures fabricated by a high-resolution 3D printer It is noteworthy that both the FEA and experiments reveal the structure with $Q = 3.6$ has significantly better performance than the structure with $Q = 6$ both in terms of the properties of vibration isolation and energy absorption. The remarkable result of this work shows its potential in choosing the layouts of multistable mechanical metamaterials.

1. Introduction

In recent decades, mechanical metamaterials, which are obtained via artificial design of internal structures without relying on manufacturing materials [1–4], have attracted a lot of attention because of their peculiar properties that are unusual in the natural world. These properties include negative Poisson's ratio [5–8] and negative stiffness [9–12]. The remarkable vibration isolation, enhanced sensitivity, and repeatable energy absorption performance of the negative stiffness structures have extended their applications in motion- and energy-related fields [13–15].

The negative stiffness of structures resulting from compression, bending, and buckling of the beam of the unit cell have been found in many structures but in different layouts. Vangbo et al. [16] first designed a "pre-compressed" slender beam and studied the snap-through phenomenon when a vertical force applied to the middle of this beam. Qiu et al. [17] directly proposed a curved beam, the shape of which is the first-order buckling mode of a straight beam. This beam does not need to rely on residual stress. The relationship between the normalized force and displacement of the middle of the beam was theoretically predicted using bucking modal superposition. They found that the bistable property of the beam can be designed and triggered by adjusting its geometric parameters. The switch between two different stabilized configurations in bistable structure has provided its applicability to serve as threshold switches, relays, shock sensors, and memory cells in microelectromechanical systems (MEMS) devices [18,19].

With the development of manufacturing technology, especially the emergence of 3D printing technology, many multistable metastructures with curved beams as the main components can be designed and manufactured [20–29]. Shan et al. [20] introduced 2D and 3D energy-trapping metamaterials using designed beam elements, and these materials are stable at the deformed state and have the property of energy dissipation. Restrepo et al. [21] designed a phase transforming cellular material that was based on a bistable curved beam. This structure can completely recover to the original shape after loading–unloading. They studied the energy absorption performance of the cellular material and found that it increases with an increase in the number of layers. Hua et al. [22] studied the influence of the out-of-plane curvature of such curved beam on its bistable characteristics from theoretical and FEA aspects, and proposed a criterion for this type of beam to achieve bistable behavior. Goldsberry

* Corresponding authors.
E-mail addresses: leihongshuai@pku.edu.cn (H. Lei), cfgao@nuaa.edu.cn (C.-F. Gao), guoxg@bit.edu.cn (X. Guo).

https://doi.org/10.1016/j.eml.2020.100640
2352-4316/

et al. [23] designed a negative stiffness honeycomb that consisted of a doubly periodic array of centrally-clamped parallel-beam and studied the propagation of elastic waves. Luo et al. [24] introduced a bistable cross-shaped structure and proposed an analytic model using a perturbation method to reveal its mechanical properties. The influence of the geometric parameters on the bistability of this structure is also verified by the experiments and numerical simulations. Ha et al. [25] used straight incline beams as the main component and introduced a negative stiffness lattice that was comprised of multiple unit cells. They analyzed the influences of the inclined angle and the beam slenderness ratio on the snap-through property.

In addition to the buckled beam, scholars have also designed some multistable structures using other mechanisms, such as latch-lock mechanisms [30], hinged multisegment mechanisms [31]. Haghpanah et al. [31] proposed a method for designing 1D, 2D, and 3D multistable shape reconfigurable materials based on living hinges. These multistable structures can also return to their original shape, and the energy absorption is reused. Fu et al. [32] used a combination of compliant stretchable components and some rigid granular materials as a new mechanism to design a multistable metamaterial. Hewage et al. [9] and Rafsanjani et al. [33] each designed mechanical metamaterials that have both negative stiffness and negative Poisson's. Yang et al. [34] created a soft structure that has a shape memory property using macroscopic and mesoscopic elastic instability.

As expected, most multistable metamaterials in porous configuration have relatively light mass. The strategy to determine the optimal set of parameters to achieve the best mechanical properties within a restricted volume is very important but is rarely reported. Furthermore, the energy can be absorbed by the reusable multilayer multistable is much smaller than the disposable plastic energy-absorbing structure with the same relative mass. Therefore, it is important to study how to improve the peak force and energy absorption efficiency of the multistable structures. In this work, we investigate the effects of parameters on the mechanical properties of a typical multistable metamaterial theoretically and numerically. When keeping the maximum strain of the unit cells constant during deflection, the results suggest that the unit cell can achieve the largest peak force and best energy absorption performance by adjusting its geometrical parameters. On the basis of the unit cell analysis, two different multilayer structures were fabricated using a stereo lithography apparatus (SLA) 3D printer. Axial compressive loading–unloading tests and numerical simulations on these structures are carried out, and the results reveal the significance of choosing the proper parameters.

2. Theoretical analysis and experimental tests

Fig. 1 shows the illustration of multilayers structure and one unit cell of the multistable metamaterial. The unit cell can be simplified into a cosine-shaped beam and some stiffening walls. The parameters that determined the layout of the cosine-shaped beam are marked in Fig. 1, where t, b, h, and l are the thickness, width, height, and span of the cosine-shaped beam respectively. Based on the assumption of clamp at two ends and limited rotation at midpoint, the configuration of the neutral axis of the curved beam can be predicted by:

$$w = \frac{h}{2}[1 + \cos(\frac{2\pi x}{l})] + \frac{t}{2}, \quad x \in [-\frac{\pi}{2}, \frac{\pi}{2}]. \tag{1}$$

This beam can be switched to another stable position by applying a vertical external force on the middle of the beam. Qiu et al. [17] used a theoretical approach and studied the effects of the parameters of the beam on its bistable mechanism. The focus of our research is on how to choose the geometric parameters of the multistable metamaterial to achieve the largest peak force and the best energy absorption performance.

2.1. Theoretical analysis for a unit cell model

The relationship between the normalized vertical force and displacement of this cosine-shaped curved beam can be expressed as follows [17]:

$$\text{model 1}: F = \frac{3\pi^4 Q^2}{2}\Delta\left(\Delta - \frac{3}{2} + \sqrt{\frac{1}{4} - \frac{4}{3Q^2}}\right) \times \left(\Delta - \frac{3}{2} - \sqrt{\frac{1}{4} - \frac{4}{3Q^2}}\right) \tag{2}$$

$$\text{model 3}: F = 8\pi^4 - 6\pi^4\Delta$$

$$F = \frac{fl^3}{EIh}, \Delta = \frac{d}{h}$$

where f is the vertical external force, d is the deflection of the center of the beam, F and Δ are the normalized force (f) and displacement (d), E is Young's modulus of the raw material, I is the area moment of inertia of the beam, and Q defined as $Q = h/t$.

In several engineering applications, the main requirement for multistable mechanical metamaterials is having a large peak force to isolate the vibration. As seen from Eq. (2), the normalized force, $F(Q)$, is only determined by the parameter Q. The external force, f, increases with a decrease in l if the other parameters remain constant. Therefore, to improve the peak force, we need to choose a shorter value of l. However, if l is too short, it will easily lead to brittle failure of the beam. The maximum strain of the cosine-shaped beam during deflection can be estimated using the following expression [17]:

$$\varepsilon_{\max} \approx 2\pi^2\frac{th}{l^2} + 4\pi^2\frac{t^2}{3l^2} = \pi^2\frac{t^2}{l^2}\left(2Q + \frac{4}{3}\right) \tag{3}$$

In engineering applications, it can be considered that the length, width, and height of the multi-stable structure are restricted values. The height and width do not limit the design of the unit cell because the parameters of the unit cell can be adjusted proportionally to meet the size of the overall structure. Thus, it makes more sense to discuss the peak force per length of the curved beam. We define the average force, f_a, that is provided by the beam as follows:

$$f_a(Q) = \frac{f}{l} = \frac{F(Q)EIh}{l^4} \tag{4}$$

Combining Eqs. (3) and (4) leads to the following:

$$f_a(Q) = \frac{{\varepsilon_{\max}}^2 Eb}{12\pi^4} \cdot \frac{F(Q)}{4Q + \frac{16}{3} + \frac{16}{9Q}} \tag{5}$$

$\varepsilon_{\max}$ is kept constant and does not exceed the yield strain of the material for each unit cell with different parameters Q. Maximum and minimum values of $F(Q)$ can be obtained by finding the intersection of two types of curves in Eq. (2):

$$\frac{3\pi^4 Q^2}{2}\Delta\left(\Delta - \frac{3}{2} + \sqrt{\frac{1}{4} - \frac{4}{3Q^2}}\right)\left(\Delta - \frac{3}{2} - \sqrt{\frac{1}{4} - \frac{4}{3Q^2}}\right) = 8\pi^4 - 6\pi^4\Delta \tag{6}$$

The three intersections are:

$$\Delta_1 = -\sqrt{1 - \frac{16}{3Q^2}} + 1, \Delta_2 = 1, \Delta_3 = \sqrt{1 - \frac{16}{3Q^2}} + 1 \tag{7}$$

The normalized maximum value of $F(Q)$ is taken at Δ_1, and combining Eqs. (2) and (5) with the first expression of Eq. (7) leads to the following:

$$f_a(Q) = \frac{\left(1 + 3 * \sqrt{1 - \frac{16}{3Q^2}}\right) Eb{\varepsilon_{\max}}^2}{24Q + 32 + \frac{32}{3Q}} \tag{8}$$

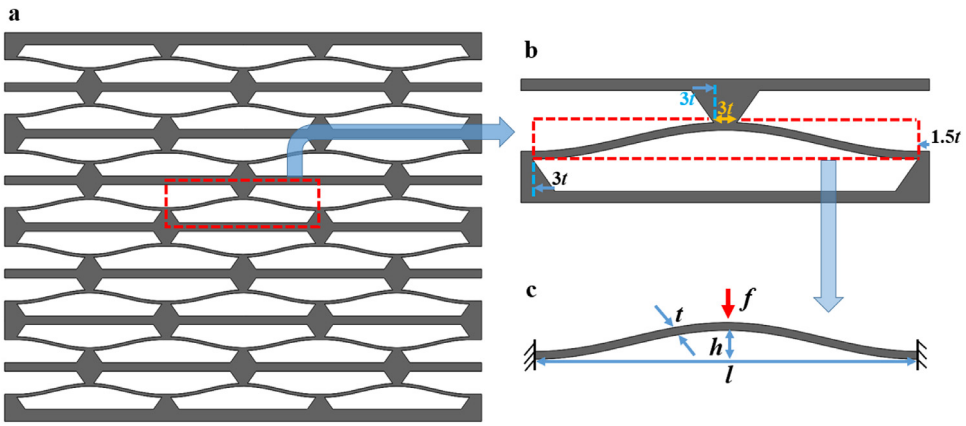

Fig. 1. Geometric configuration and parameters of the multistable metamaterial: (a) multilayer structure, (b) unit cell, and (c) cosine-shaped beam.

The derivative of function $f_a(Q)$ can then be derived using the commercial software Maple 18. We find that the maximum value of f_a is at $Q = 3.288$ in the domain of the definition, and f_{amax} is about 130% times greater than the value of f_a (6). It is worth noting the value of Q in most previous studies is generally taken as 6 or even larger than 6 [17,21,22,28], $f_a(Q)$ increases firstly and then decrease as Q increases from 2.31, and reaches its maximum value when Q is 3.288. To maximize the energy absorption in one loading–unloading cycle, the function to describe the difference between maximum and minimum forces was explored and can be given by

$$\varphi(Q) = \frac{\varepsilon_{\max}{}^2 Eb}{12\pi^4} \cdot \frac{F_{\max}(Q) - F_{\min}(Q)}{4Q + \frac{16}{3} + \frac{16}{9Q}} \tag{9}$$

By combining Eq. (2) and the first and third expressions of Eq. (7), the difference between maximum and minimum forces are expressed as:

$$F_{\max}(Q) - F_{\min}(Q) = 12\pi^4 \sqrt{1 - \frac{16}{3Q^2}} \tag{10}$$

The derivative of the function $\varphi(Q)$ is as follows:

$$\varphi'(Q) = \frac{\varepsilon_{\max}{}^2 Eb}{2} \left[\frac{16}{\sqrt{9 - \frac{48}{Q^2}\left(Q + \frac{4}{3} + \frac{4}{9Q}\right)} Q^3} - \frac{\sqrt{9 - \frac{48}{Q^2}}\left(1 - \frac{4}{9Q^2}\right)}{3\left(Q + \frac{4}{3} + \frac{4}{9Q}\right)^2} \right] \tag{11}$$

The derivative is set equal to zero, and we obtain two extreme points:

$$Q_1 = \frac{1}{3}\left(1 - \sqrt{97}\right), Q_2 = \frac{1}{3}\left(1 + \sqrt{97}\right) \tag{12}$$

The function $\varphi(Q)$ reaches its maximum value at point Q_2, and this value is 120% times greater than that of φ (6). This means that the structure has the best energy absorption effect when the value of Q is about 3.6. The function $\varphi(Q)$ increases monotonically with an increase in Q when $3.6 > Q > 2.31$, and the function $\varphi(Q)$ decreases monotonically with an increase in Q when $Q > 3.6$.

These results are very different from what was previously understood. In the later chapters of this article, the correctness of the theoretical results is verified via FEA and experimental validation.

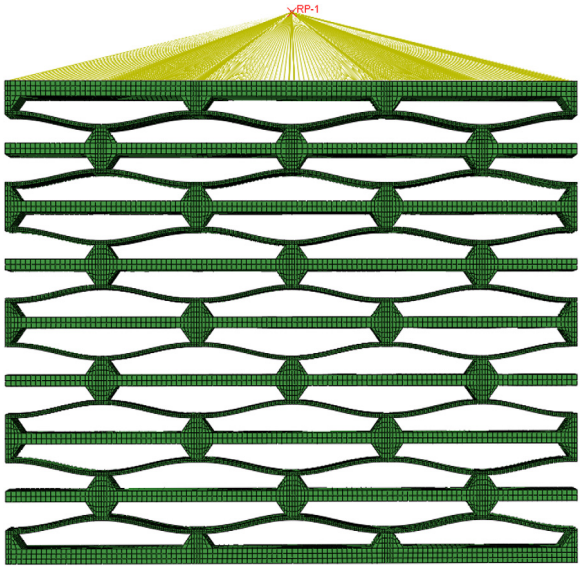

Fig. 2. Finite element model and boundary conditions of the multilayer structure.

2.2. Finite element simulation

To further analyze the influences of various parameters on the normalized force–displacement response of the unit cell and to compare the energy absorption characteristics of multilayer multistable metamaterials that have different parameters, we carried out some nonlinear finite element simulations. The FEA models were meshed using 20-node linear hexahedral elements with reduced integration (C3D20R). Mesh sensitive analysis was first carried out to ensure computational accuracy. The (Dynamics, Implicit) analysis step was employed for multilayer structures that had the optional nonlinear geometry. The geometric parameters of the multilayer structure were the same as those of the experimental specimens. The material properties were also set on the basis of experimental data. As shown in Fig. 2, the bottom of both the unit cell and multilayer structure were set as fully clamped in the boundary condition, and the prescribed displacement was applied on top of them using a kinematic coupling to link the top face with a reference point.

2.3. Experimental tests

To compare the energy absorption properties of the multilayer metamaterials that had different parameters, we fabricated two

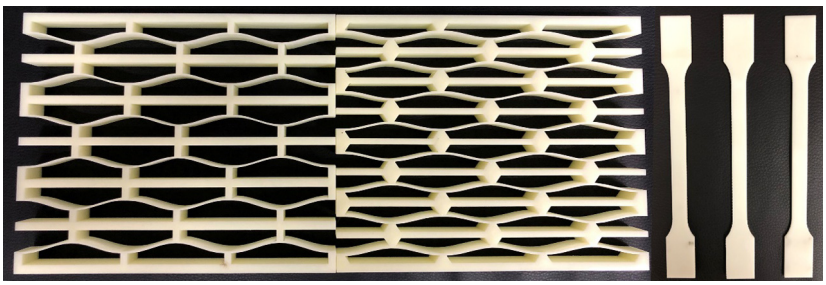

Fig. 3. Multilayer multistable structures and tensile test samples fabricated using an SLA 3D printer.

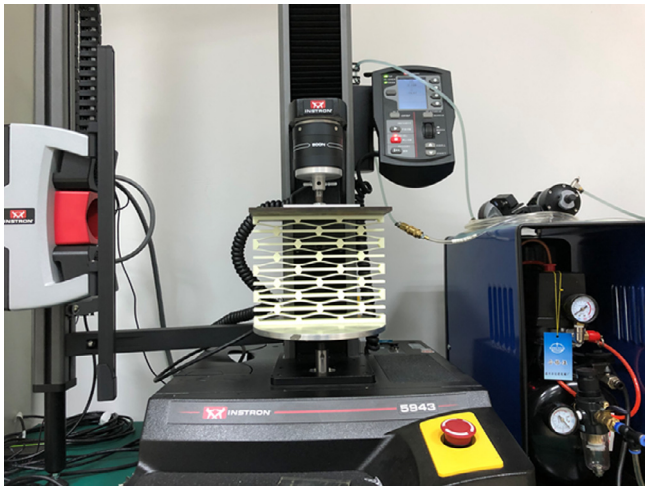

Fig. 4. Experimental setup of multi-stable structures under uniaxial compression.

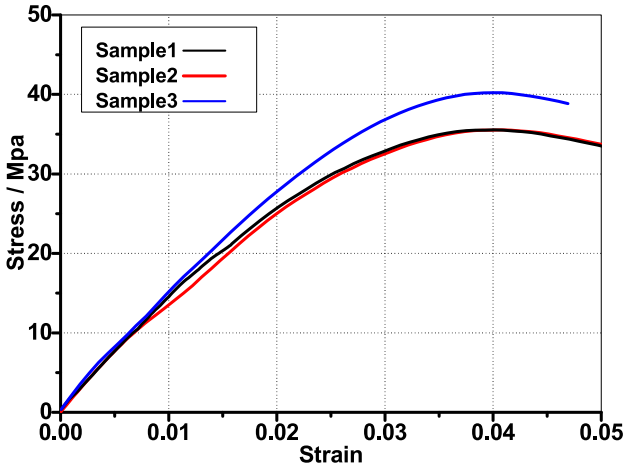

Fig. 5. Stress–strain curves obtained from tensile tests of parent material.

Table 1
Geometrical parameters of the fabricated multistable multilayer structures.

Array number	layers	b (mm)	t (mm)	h (mm)	l (mm)
3	6	10	1	6	60
3	8	10	1.25	4.5	60

different specimens using an SLA 3D printer with a high spatial resolution (5 μm) (Machine: ProJet 360; Material: VisiJet M3 Crystal). Images of the specimens are shown in Fig. 3. These two specimens have the same length (186 mm), width (20 mm), and height (161 mm). The geometrical parameters of their unit cells are listed in Table 1. Some quasi-static cyclic loading experiments in displacement–loading mode were conducted at room temperature, and the speed was set as 5 mm/min. A uniaxial testing machine (INSTRON 5943) and a video extensometer (INSTRON AVE2) were used to measure the compression force and displacement, as shown in Fig. 4. The force and displacement resolution of the loading cell were 0.0001 N and 0.0001 mm, respectively. Setting the maximum load displacement causes all of the layers of a specimen to be fully deformed. Moreover, to harvest the mechanical properties of parent material, some uniaxial tensile specimens were fabricated using the same process. According to the ASTM E8-15a standard, the uniaxial tensile loading speed was set as 1 mm/min. The typical tensile stress verse strain curves are shown in Fig. 5. The average Young's modulus of the parent material is approximately 1550 MPa. The initial yield strength and strain are about 38.5 MPa and 3.7%, respectively. The parent material exhibits excellent elastic–plastic behavior with an increase in the uniaxial strain. Multistable metamaterial structure can maintain an elastic state during the whole progress of the experiment, thus the yield parameters are not considered in the FEA model.

3. Results and discussion

3.1. Effects of geometric parameters on the snapping behavior of the unit cell

Qiu et al. [17] shows that only the geometric parameter ($Q = h/t$) of the cosine-shaped beam of the unit cell has a significant effect on the normalized force–displacement curve. Their theory is based on the assumption of small deformation. However, to obtain a larger peak force, the ratio of length to height will be a relatively small value such that the theory model based on the small deformation hypothesis is not very reasonable to predict the mechanical performances of multistable metamaterials [22, 35]. We developed series models of the unit cells for simulation and their parameter b is constant, 6 mm.

The normalized force–displacement curves of the unit cells that were obtained via FEA methods were shown in Fig. 6, as well as theoretical results. In Fig. 6(a), two FEA unit cells have the same parameters, $Q = 3$ and $t = 1$ mm, whereas their l is 60 mm and 300 mm, respectively. The unit cells in Fig. 6(b) are similar to the one used in Fig. 6(a) except their larger Q (i.e. 4). The normalized force–displacement curves of the two unit cells in both Fig. 6(a) and (b) are different, even with the same Q, and FEA results of that with a larger l are more closer to the theoretical results, resulting from its more applicable to small deformation hypothesis. In Fig. 6(c), two FEA unit cells have the

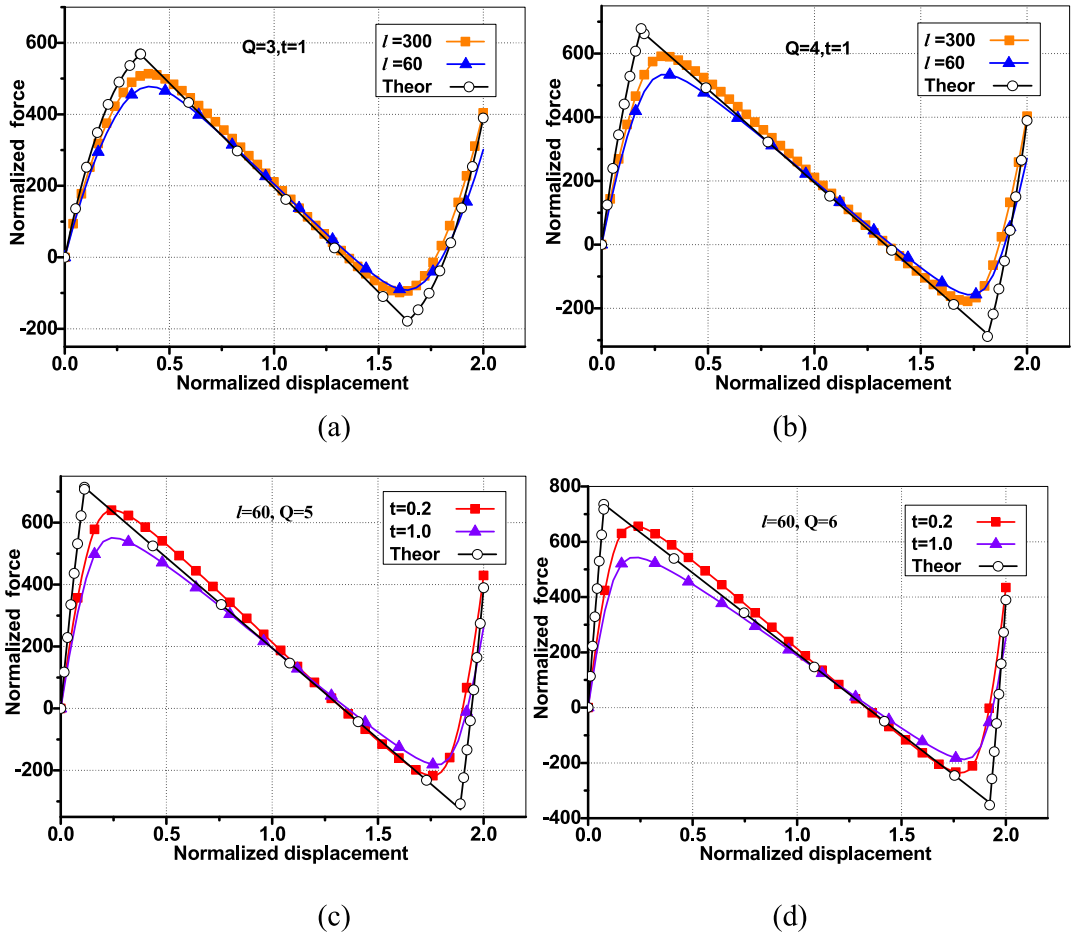

Fig. 6. Comparison of the analytical and numerical compressive responses of the unit cell structure ($b = 6$ mm): (a) ($Q = 3$, $t = 1$ mm), $l = 60$ mm, and 300 mm; (b) ($Q = 4$, $t = 1$ mm), $l = 60$ mm, and 300 mm; (c) ($l = 60$ mm, $Q = 5$), $t = 0.2$ mm, and 1.0 mm; (d) ($l = 60$ mm, $Q = 6$), $t = 0.2$ mm, and 1.0 mm.

same parameters $Q = 5$ and $l = 60$ mm, whereas their t is 0.2 mm and 1 mm, respectively. The unit cells in Fig. 6(d) are similar to the one used in Fig. 6(c), except their larger Q (i.e. 6). As seen in both of these two graphs, although Q and l remain the same, the normalized force–displacement curves of these two unit cells are still different.

The curve for the unit cell that has the thinner parameter t is closer to the theoretical result. In Fig. 7(a), we compare the results for the maximum normalized force of several unit cells as obtained using FEA to the results obtained using theoretical means. These unit cells have the same parameter $t = 1$ mm with Q values that range from 3 to 6, but the parameter l is 60 mm and 300 mm, respectively. It is clear that there is a significant difference between the FEA results and theoretical results, and this error can be as much as 24% for the unit cell with the parameter $l = 60$ mm. Moreover, the normalized force of the unit cell with $t = 1$ mm, $Q = 5$, and $l = 60$ mm is even slightly higher than that of the unit cell with $t = 1$ mm, $Q = 6$, and $l = 60$ mm.

The above conclusions show that the parameter Q has an influence on the normalized force–displacement curve of the unit cell. Another influencing factor can be defined as $P = l/h$, and the accuracy of the theoretical results decreases with a decrease in the parameter P. As shown in Fig. 7(b) and (c), we compared the normalized force–displacement curves and maximum normalized force values obtained via FEA for unit cells that have the same parameters Q and P but different t. These paired curves are almost identical, and the difference between their maximum normalized force values is only 3%. These results can be proved via a simple analysis. Consider the following two types of beams:

$$\text{Beam 1: } w_1 = \frac{Qt_1}{2}[1+\cos(\frac{2\pi x}{PQt_1})] + \frac{t_1}{2}, \quad x \in [-\frac{PQt_1}{2}, \frac{PQt_1}{2}]$$
$$\text{Beam } k\text{: } w_k = \frac{Qt_k}{2}[1+\cos(\frac{2\pi x}{PQt_k})] + \frac{t_k}{2}, \quad x \in [-\frac{PQt_k}{2}, \frac{PQt_k}{2}] \tag{13}$$

It is obvious that the normalized force–displacement curves of beam k are the same as that of beam 1, and the simple proof of this is as follows:

$$F_1 = \frac{f_1 l_1^3}{E_1 I_1 h_1} = \frac{12 f_1 P^3 Q^2}{E_1 b t_1} = \frac{12\left(f_1 \cdot \frac{t_2}{t_1}\right) P^3 Q^2}{E_1 b t_2} = \frac{f_k l_k^3}{E_1 I_k h_k} = F_k \tag{14}$$

This means that if the parameters Q and P are the same for different unit cells, the unit cells have the same normalized force–displacement curve. This property is still applicable for large deformation situations. On the basis of this, we can keep t constant and studied the effects of changes in Q and P on the properties of the unit cell. We developed a series of FEA unit cell models with the same parameter $t = 1$ mm and kept their $\varepsilon_{\max}$ value equal to 3.65%. This 3.65% value is the maximum strain of the unit cell that has the parameters $l = 60$ mm, $t = 1$ mm, and $h = 6$ mm during deflection. This strain in the elastic range of the material is that we used for 3D printing. The values of Q for these unit cells are 2.5, 2.7, 3, 3.2, 3.4, 3.6, 3.8, 4, 4.5, 5,

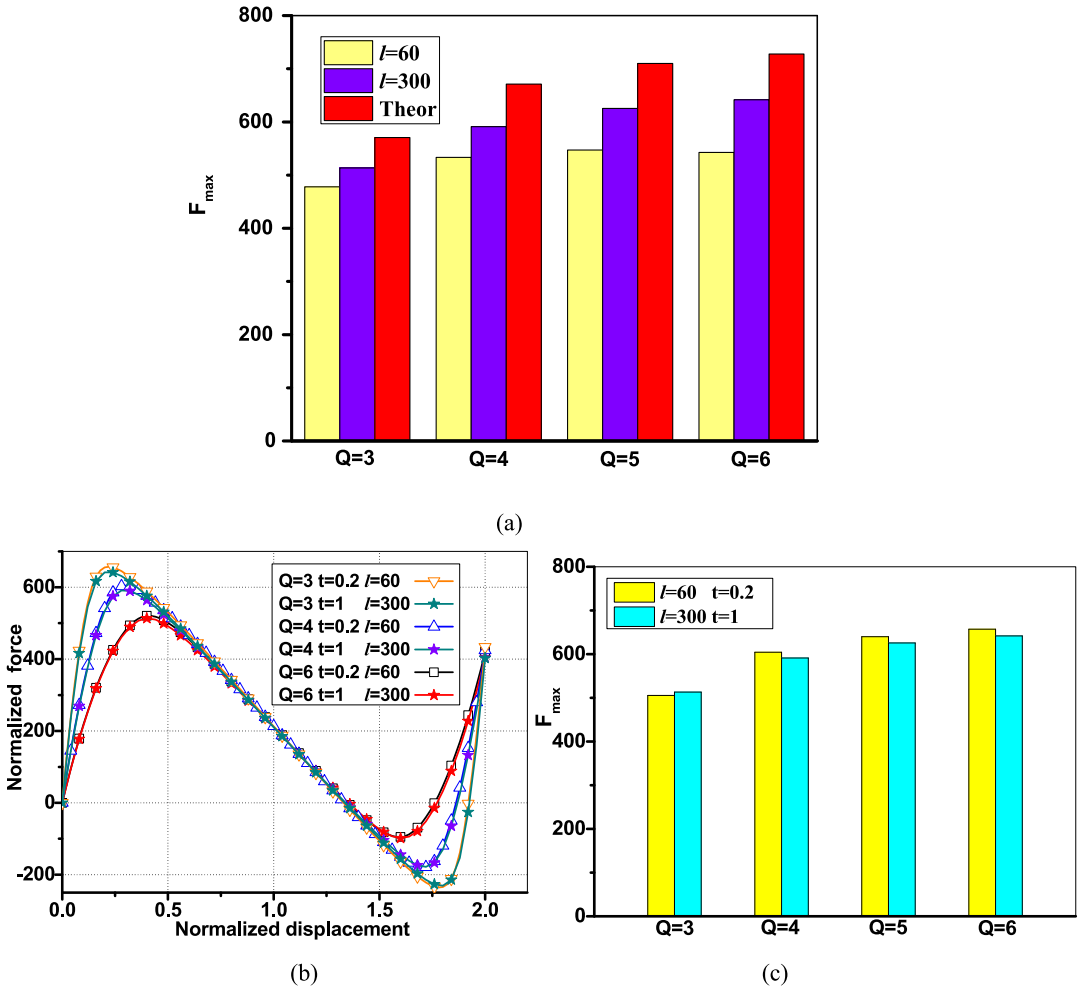

Fig. 7. Comparison of the maximum normalized force for unit cell with different parameters as obtained from theoretical and FEA results: (a) ($t = 1$ mm, $b = 6$ mm), Q range from 3 to 6, $l = 60$ mm and 300 mm; (b) and (c) comparison of normalized F-D curves and maximum force of the unit cell with different parameters as ($P = 300$, $b = 6$ mm), Q range from 3 to 6, $t = 0.2$ mm and $t = 1$ mm.

5.5, and 6. Their length, l, is determined by Eq. (3). As seen in Fig. 8(a) and (b), we compared the peak forces per length (f_{amax}) and the determinant of the energy absorption efficiency ($\varphi(Q)$) as obtained from FEA and theoretical results. The FEA results of f_{amax} and $\varphi(Q)$ reach their maximum values at $Q = 3.1$ and $Q = 3.5$, respectively, and these are close to the theoretical results. These FEA values are both about 140% times of the corresponding $f_a(6)$ and $\varphi(6)$ values. Although there are differences between the FEA and theoretical values, their trends are basically similar and it makes more sense to know how to choose the parameters to achieve the corresponding maximum value instead of finding the maximum value. These differences are due to the theoretical analysis is based on the small deformation hypothesis, the approximation is less accurate when parameter $P(l/h)$ is small. Moreover, to obtain larger peak force and better energy absorption efficiency, the designed parameters $P(l/h)$ for these FEA models cannot larger enough. However, compared to the yield strain values of many materials, 3.65% is a relatively large strain, and this means that our results are applicable for most range of engineering applications using multistable structures.

3.2. Energy absorption comparison for multilayer metastructures that have different parameters

In the above sections, we discussed how to determine parameters to maximize the peak forces per length and the energy absorption efficiency based on the FEA and theoretical results. On the basis of this and for further verification, two different multilayer metastructures were fabricated, as shown in Fig. 3. These specimens have the same length, width and height. Their unit cell has the same maximum strain during its deflection. The structure with $Q = 6$ uses the same stiffening wall as that reported by Restrepo et al. [21], whereas the structure with $Q = 3.6$ uses the stiffening wall shown in Fig. 1. To reveal their snap-through behavior and energy dissipation property, both FEA simulations and experimental tests were conducted, and the results are compared in Fig. 9. The deformation processes including the complete loading–unloading process. The geometrical and material mechanical parameters of the FEA models were determined from the experimental results.

Both of the two multilayer structures exhibit evident snap-through and energy absorption behaviors (Fig. 9). There was an obvious energy dissipation region between the loading the unloading curves. For the multilayer structures, with the increase in compressive displacement, one of the layers achieves its peak force first and then turns into another bistable position, resulting in the phenomenon of snap-through. For the specific deformation details of structures with $Q = 3.6$, readers are referred to the movies (M1-experiment and M2-FEA) provided in the supplemental materials. The structure can be stabilized at this position after the compressive load is removed. After unloading, the structure also recovers to the initial configuration, and this

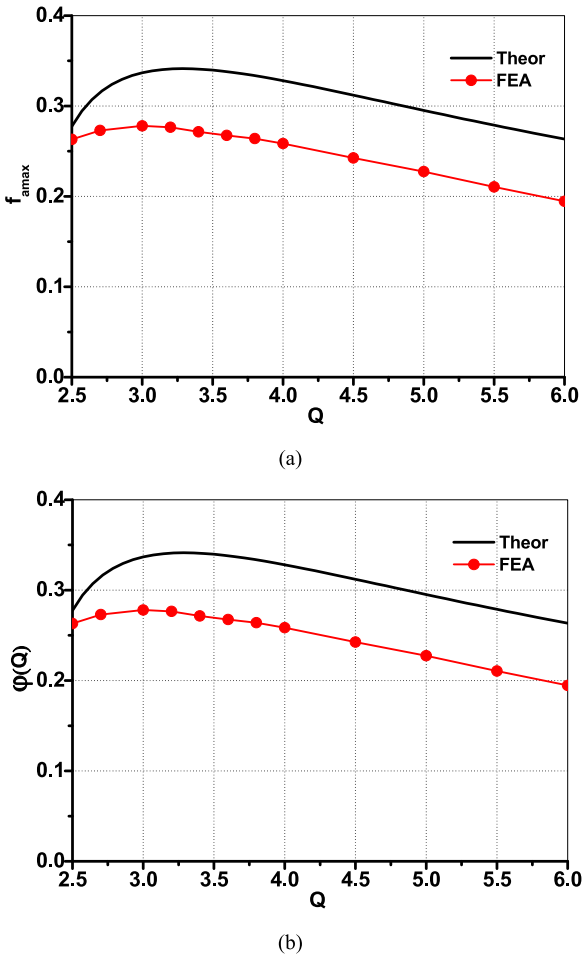

Fig. 8. Effects of parameter Q on the peak force per length (f_{amax}) and the determinant of the energy absorption efficiency ($\varphi(Q)$) of the unit cell when maximum strain is kept at 3.65%.

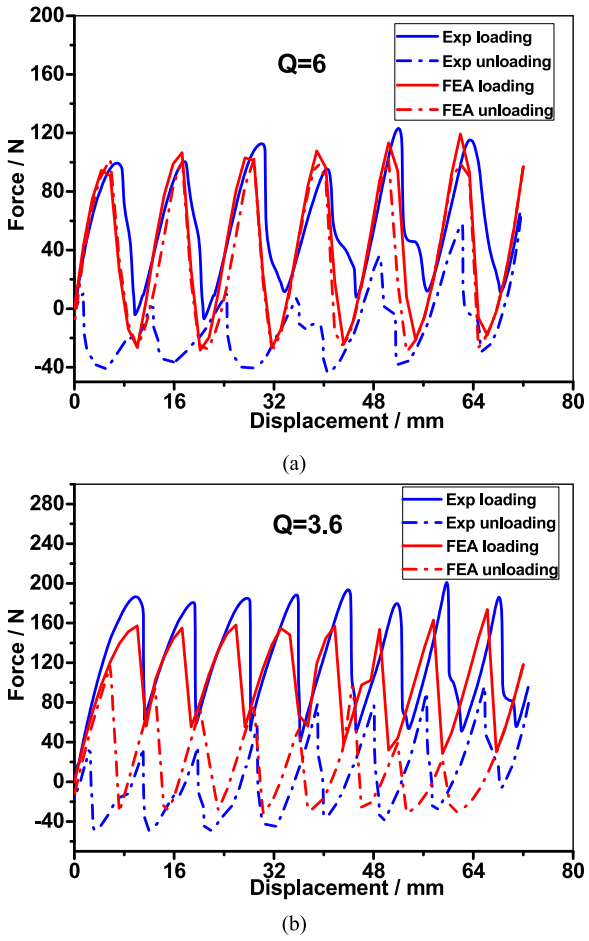

Fig. 9. Numerical and experimental axial force–displacement relationships of multilayer structures with $Q = 3.6$ and $Q = 6$: (a) $Q = 6$, experimental and FEA results; (b) $Q = 3.6$, experimental and FEA results.

means that the structure can be reused. The snap-through times of each multilayer structure are equal to their numbers of layers both during the loading and unloading processes.

In the loading process, the FEA results agree well with experiments, especially in the terms of peak force and the threshold displacement of the phase transition. Also, the maximum discrepancy of the structures with $Q = 3.6$ and $Q = 6$ are less than 15% and 5%, respectively. The multistructure with $Q = 3.6$ shows its advantage in energy absorption for its larger region in the loading and unloading curves compared with $Q = 6$. Meanwhile, the snap-through process for the structure with $Q = 3.6$ is more smooth, resulting from its stronger stiffening walls. Another main factor is that the structure with $Q = 3.6$ has more layers [21,22,25]. Keeping the overall structure size constant and reducing the parameter size of the two unit cells in proportion can increase the number of layers, and thus can improve the energy absorption characteristics of the structure. When the number of layers of these two kinds of structures is large enough, their energy absorption performance can be considered as only determined by the maximum peak force because their displacements are the same [21]. However, the experimental peak force of the structure with $Q = 3.6$ is obviously greater than that of another structure, and the ratio is about 150%. This means that the energy absorption capacity of the structure with $Q = 3.6$ is at least 50% higher than the structure with $Q = 6$ no matter how many layers the structure has.

During the unloading process, the FEA force–displacement curve of the structure with $Q = 6$ is obviously different compared to experimental results. The FEA unloading curve is almost the same as the loading curve, because it does not meet the condition [21]:

$$\left(\frac{n_{\mathrm{I}}}{k_{\mathrm{I}}}+\frac{n_{\mathrm{III}}}{k_{\mathrm{III}}}\right)^{-1} \leq |k_{\mathrm{II}}| \tag{15}$$

where k_I, k_{II}, and k_{III} are stiffness coefficients of the three linear segments that pass through four points: (0,0), (Δ_1, $F(\Delta_1)$), (Δ_3, $F(\Delta_3)$), and (2, $F(2)$); n_I and n_{III} are the numbers of layers per structure in regimes k_I and k_{III}, respectively. However, the experimental unloading curve is different from the experimental loading curve, and this can be ascribed to the influence of the viscoelasticity of the resin material for the 3D-printed sample [25,28]. Moreover, the structure with $Q = 3.6$ satisfies Eq. (15), and thus, its FEA loading–unloading curves enclose a closed area even when the material is elastic. This also reflects the importance of choosing appropriate parameters.

4. Conclusions

In summary, we further studied a typical multistable mechanical metamaterial and strengthened its stiffening wall. We analyzed the effects of the geometric parameters of the unit cell on its mechanical properties by combined theoretical modeling

and numerical simulations. For unit cells with the same maximum strain during deflection, the results show that we can obtain the largest peak force and best energy absorption performance by adjusting the geometrical parameters. Furthermore, the unit cells with the same parameters Q and P have the same normalized force–displacement curve no matter for small deformation or large deformation. Moreover, we numerically and experimentally studied the mechanical response of two different multilayer structures fabricated by a high-resolution 3D printer. The results showed that the structure with $Q = 3.6$ has better performance than the structure with $Q = 6$ on both the properties of vibration isolation and energy absorption. This work subverts some of our conventional ideas and has a guiding effect on the design of a variety of multistable structures, especially those used for some specific engineering problems.

Declaration of competing interest

The authors declare that they have no known competing financial interests or personal relationships that could have appeared to influence the work reported in this paper.

Acknowledgments

This work was supported by the National Key Research and Development of China (2017YFB0103801), the National Natural Science Foundation of China (11872012, 11472130 and 11702131), and the Young Elite Scientists Sponsorship Program, PR China.

Appendix A. Supplementary data

Supplementary material related to this article can be found online at https://doi.org/10.1016/j.eml.2020.100640.

References

[1] H. Fang, S.A. Chu, Y. Xia, K.W. Wang, Programmable self-locking origami mechanical metamaterials, Adv. Mater. 30 (15) (2018) 1706311.
[2] Y. Zhang, F. Zhang, Z. Yan, Q. Ma, X. Li, Y. Huang, et al., Printing, folding and assembly methods for forming 3D mesostructures in advanced materials, Nat. Rev. Mater. 2 (4) (2017) 17019.
[3] X. Yu, J. Zhou, H. Liang, Z. Jiang, L. Wu, Mechanical metamaterials associated with stiffness, rigidity and compressibility: a brief review, Prog. Mater. Sci. 94 (2017) 114–173.
[4] L. Meza, S. Das, J. Greer, Strong, lightweight, and recoverable three-dimensional ceramic nanolattices, Science 345 (6202) (2014) 1322–1326.
[5] C. Ma, H. Lei, J. Hua, Y. Bai, J. Liang, D. Fang, Experimental and simulation investigation of the reversible bi-directional twisting response of tetra-chiral cylindrical shells, Compos. Struct. 203 (2018) 142–152.
[6] R. Lakes, Foam structures with a negative Poisson's ratio, Science 235 (4792) (1987) 1038–1040.
[7] K. Bertoldi, P. Reis, S. Willshaw, T. Mullin, Negative Poisson's ratio behavior induced by an elastic instability, Adv. Mater. 22 (3) (2010) 361–366.
[8] Q. Ma, H. Cheng, K. Jang, H. Luan, K. Hwang, J. Rogers, Y. Huang, Y. Zhang, A nonlinear mechanics model of bio-inspired hierarchical lattice materials consisting of horseshoe microstructures, J. Mech. Phys. Solids 90 (2016) 179–202.
[9] T. Hewage, K. Alderson, A. Alderson, F. Scarpa, Double-negative mechanical metamaterials displaying simultaneous negative stiffness and negative Poisson's ratio properties, Adv. Mater. 28 (46) (2016) 10323–10332.
[10] R. Lakes, W. Drugan, Dramatically stiffer elastic composite materials due to a negative stiffness phase, J. Mech. Phys. Solids 50 (5) (2002) 979–1009.
[11] B. Haghpanah, L. Salarisharif, P. Pourrajab, J.B. Hopkins, L. Valdevit, Multistable shape-reconfigurable architected materials, Adv. Mater. 28 (36) (2016) 7915–7920.
[12] Y. Jiang, L.M. Korpas, J.R. Raney, Bifurcation-based embodied logic and autonomous actuation, Nature Commun. 10 (1) (2019) 128.
[13] M. Caruel, J. Allain, L. Truskinovsky, Mechanics of collective unfolding, J. Mech. Phys. Solids 76 (2015) 237–259.
[14] E. Duoss, T. Weisgraber, K. Hearon, C. Zhu, W. Small, T. Metz, J. Vericella, H. Barth, J. Kuntz, R. Maxwell, C. Spadaccini, T. Wilson, Three-dimensional printing of elastomeric, cellular architectures with negative stiffness, Adv. Funct. Mater. 24 (31) (2014) 4905–4913.
[15] N. Hu, R. Burgueno, Buckling-induced smart applications: recent advances and trends, Smart Mater. Struct. 24 (6) (2015) 063001.
[16] M. Vangbo, An analytical analysis of a compressed bistable buckled beam, Sensors Actuators A 69 (3) (1998) 212–216.
[17] J. Qiu, J. Lang, A.H. Slocum, A curved-beam bistable mechanism, J. Microelectromech. Syst. 13 (2) (2004) 137–146.
[18] I. Hwang, Y. Shim, J. Lee, Modeling and experimental characterization of the chevron-type bi-stable microactuator, J. Micromech. Microeng. 13 (6) (2003) 948–954.
[19] M. Capanu, J.G. Boyd, P.J. Hesketh, Design, fabrication, and testing of a bistable electromagnetically actuated microvalve, J. Micro. Electromech. Syst. 9 (2) (2000) 181–189.
[20] S. Shan, S. Kang, J. Raney, P. Wang, L. Fang, F. Candido, J. Lewis, K. Bertoldi, Multistable architected materials for trapping elastic strain energy, Adv. Mater. 27 (29) (2015) 4296–4301.
[21] D. Restrepo, N.D. Mankame, P.D. Zavattieri, Phase transforming cellular materials, Extreme Mech. Lett. 4 (2015) 52–60.
[22] J. Hua, H. Lei, Z. Zhang, C. Gao, D. Fang, Multistable cylindrical mechanical metastructures: Theoretical and experimental studies, J. Appl. Mech. 86 (7) (2019) 1–27.
[23] B. Goldsberry, M. Haberman, Negative stiffness honeycombs as tunable elastic metamaterials, J. Appl. Phys. 123 (9) (2018) 091711.
[24] G. Luo, H. Fu, X. Cheng, K. Bai, L. Shi, X. He, J. Rogers, Y. Huang, Y. Zhang, Mechanics of bistable cross-shaped structures through loading-path controlled 3D assembly, J. Mech. Phys. Solids. 129 (2019) 261–277.
[25] C. Ha, R. Lakes, M. Plesha, Design, fabrication, and analysis of lattice exhibiting energy absorption via snap-through behavior, Mater. Des. 141 (2018) 426–437.
[26] A. Rafsanjani, A. Akbarzadeh, D. Pasini, Snapping mechanical metamaterials under tension, Adv. Mater. 27 (39) (2015) 5931–5935.
[27] H. Yang, L. Ma, Multi-stable mechanical metamaterials with shape-reconfiguration and zero Poisson's ratio, Mater. Des. 152 (2018) 181–190.
[28] K. Che, C. Yuan, J. Wu, H. Qi, J. Meaud, Three-dimensional-printed multistable mechanical metamaterials with a deterministic deformation sequence, J. Appl. Mech. 84 (1) (2017) 0111004.
[29] S. Liu, A.I. Azad, R. Burgueño, Architected materials for tailorable shear behavior with energy dissipation, Extreme Mech. Lett. 28 (2019) 1–7.
[30] M. Hoffmann, P. Kopka, E. Voges, All-silicon bistable micromechanical fiber switch based on advanced bulk micromachining, J. Sel. Top. Quant. 5 (1) (1999) 46–51.
[31] B. Haghpanah, L. Salari-Sharif, P. Pourrajab, J. Hopkins, L. Valdevit, Multistable shape-reconfigurable architected materials, Adv. Mater. 28 (36) (2016) 7915–7920.
[32] K. Fu, Z. Zhao, L. Jin, Programmable granular metamaterials for reusable energy absorption, Adv. Funct. Mater. 29 (32) (2019) 1901258.
[33] A. Rafsanjani, D. Pasini, Bistable auxetic mechanical metamaterials inspired by ancient geometric motifs, Extreme Mech. Lett. 9 (2016) 291–296.
[34] D. Yang, L. Jin, R.V. Martinez, K. Bertoldi, G. Whitesides, Z. Suo, Phase-transforming and switchable metamaterials, Extreme Mech. Lett. 6 (2016) 1–9.
[35] M. Alturki, R. Burgueño, Response characterization of multistable shallow domes with cosine-curved profile, Thin-Walled Struct. 140 (2019) 74–84.